EXPERIMENTAL ASSESSMENT OF THE FUEL HEATING AND THE VALIDITY OF THE ASSUMPTION OF ADIABATIC FLOW THROUGH THE INTERNAL ORIFICES OF A DIESEL INJECTOR

Salvador, F.J., Gimeno, J., Carreres, M. (*), Crialesi-Esposito, M.

CMT-Motores Térmicos, Universitat Politècnica de València

Camino de Vera s/n, E-46022 Spain

(*) Corresponding author:

Mr. Marcos Carreres, marcarta@mot.upv.es

CMT-Motores Térmicos, Universitat Politècnica de València

Camino de Vera s/n, E-46022 Spain

Telephone: +34-963876540

Fax: +34-963877659

ABSTRACT

In this paper an experimental investigation on the heating experienced by the fuel when it expands through the calibrated orifices of a diesel injector is carried out. Five different geometries corresponding to the control orifices of two different commercial common-rail solenoid injectors were tested. An experimental facility was used to impose a continuous flow through the orifices by controlling the pressures both upstream and downstream of the restriction. Fuel temperature was controlled prior to the orifice inlet and measured after the outlet at a location where the flow is already slowed down. Results were compared to the theoretical temperature increase under the assumption of adiabatic flow (i.e. isenthalpic process). The comparison points out that this assumption allows to predict the fuel temperature change in a reasonable way for four of the five geometries as long as the pressure difference across the orifice is high enough. The deviations for low imposed pressure differences and the remaining orifice are explained due to the low Reynolds numbers (i.e. flow velocities) induced in these cases, which significantly increase the residence time of a fuel particle in the duct, thus enabling heat transfer with the surrounding atmosphere. A dimensionless parameter to quantify the proneness of the flow through an orifice to exchange heat with the surroundings has been theoretically derived and calculated for the different geometries tested, allowing to establish a boundary that defines beforehand the conditions from which heat losses to the ambient can be neglected when dealing with the internal flow along a diesel injector.

Salvador, F.J., Gimeno, J., Carreres, M., Crialesi-Esposito, M., "Experimental assessment of the fuel heating and the validity of the assumption of adiabatic flow through the internal orifices of a diesel injector".

Fuel 188 (2017), pp. 442-451 (author version)

KEYWORDS

diesel, experimental, fuel heating, fuel temperature, adiabatic flow

LIST OF NOTATION

A_o	outlet area
A_P	area submitted to heat transfer
Ad	adiabatic number
C_d	discharge coefficient
c_p	fluid heat capacity at constant pressure
D_i	inlet diameter
D_o	outlet diameter
e	specific internal energy
h	specific enthalpy
k	thermal conductivity
L	length
$\dot{m}$	mass flow
$\dot{m}_{th}$	theoretical mass flow
Nu	Nusselt number
p	pressure
p_0	reference pressure
p_{dw}	downstream pressure
p_{up}	upstream pressure
p_v	vapour pressure
P	perimeter
Pr	Prandtl number
$\dot{q}$	heat flux
Re	Reynolds number
Re_{crit}	critical Reynolds number
St	Stanton number
T	temperature

T_0 reference temperature

T_{dw} downstream temperature

T_f fluid temperature

T_{up} upstream temperature

T_w wall temperature

u flow velocity

u_m mean flow velocity

u_{th} theoretical flow velocity

GREEK SYMBOLS:

α convective heat transfer coefficient

β volumetric thermal expansion coefficient

Δp pressure drop

ΔT temperature change

ΔT_{exp} experimental temperature change

ΔT_{th} theoretical temperature change

μ absolute viscosity

μ_b absolute viscosity evaluated at the bulk temperature

μ_w absolute viscosity evaluated at the wall

ρ density

1. INTRODUCTION

Based on the attention it has been given by researchers in the diesel engine community, the direct injection system is one of the key elements on the engine's outcome. It is directly related to the air-fuel mixture quality [1][2][3], which results in a strong influence on the combustion phenomenon, thus affecting the fuel consumption and emissions [4][5][6][7]. Advancements in the direct injection systems features have been used as a vehicle to reduce both soot and NO_x emissions in order to meet the restrictive requirements of the Euro 6 legislation and those to come. As a result, for instance, the injection pressure realizable by the injection systems is growing at a fast rate, already reaching 250 or 300 MPa. This results in a higher complexity of the injection system, which highlights the need for advanced tools that allow to predict its behaviour at the wide range of engine operating conditions [8].

It is therefore important to develop computational tools to simulate the internal flow through injector systems. Approaches have been made through one-dimensional modelling of the complete injector flow [9][10][11][12][13][14] or three-dimensional modelling of the nozzle flow [4][15][16][17][18]. Some of these works assume that the flow is isothermal [11][12][13][14]. Nevertheless, the raising injection pressures may also induce relevant fuel temperature changes due to friction heating or due to important fuel depressurization across the injector control orifices or the nozzle [15][16]. These fuel temperature changes, in turn, affect the fuel properties, which are strongly dependant on temperature and pressure [19][20][21][22][23]. For this reason, some modellers prefer to assume the flow along the injector as adiabatic [9][10]. However, attention has never been given to the validation of this hypothesis, which may not be true under some real circumstances. Even though the temperature difference among the fuel and the injector walls may be high, heat transfer to the surroundings is not expected to be relevant if the flow velocity is high enough to lead to low residence times of a fuel particle within the injector. However, the adiabatic assumption may not hold if the fuel velocity is too low and there is enough time for the fuel to interact with the ambient.

The purpose of this work is to shed light on the previous issues by having a look at the flow through the most important restrictions in diesel injectors from an experimental point of view. Continuous flow through the two control orifices of a Bosch CRI 2.20 injector (described in [23]) and the three control orifices of a Denso G4S (which uses a three-way valve to hydraulically pilot the injector, as described in [24]) was established for different imposed pressure drops, making it possible to measure the generated increase in temperature. Results were compared to the theoretical temperature increase expected if the expansion through the orifice was isenthalpic, which includes the assumption of adiabatic flow. An analysis of the deviations in temperature increase between the experiments and the theoretical isenthalpic process was performed in order to establish the conditions under which the assumption of adiabatic flow through a diesel injector is valid. In this regard, a dimensionless parameter was defined in order to condense the information of the five tested orifices in a single parameter that quantifies the proneness of a certain orifice to exchange heat with the surroundings when working under specific conditions.

2. THEORETICAL TEMPERATURE CHANGE FOR AN ISENTHALPIC PROCESS

As it has been stated, the experimental results of the temperature change across the orifice upon expansion will be compared to the theoretical temperature change predicted under the assumption of adiabatic flow, with no heat transfer to the surroundings. According to the first law and in the absence of external work, this assumption implies that the stagnation enthalpy is conserved along the orifice:

$$\Delta\left(h+\frac{1}{2}u^2\right)=0 \tag{1}$$

Furthermore, if the reference locations upstream and downstream of the orifice at which the pressure is controlled are placed far enough from the orifice (so as to assume that the flow velocity is similar at those locations), the specific enthalpy of the flow is supposed to remain constant along the process carried out in the experiments. Then, under these conditions, the flow may be regarded to as isenthalpic.

The relationship among the specific enthalpy of the flow and its internal energy is given by Eq. (2):

$$h=e+\frac{p}{\rho} \tag{2}$$

It is important to note that, due to the small diameters involved in the study, the heating induced by viscous dissipation (i.e. friction) along the orifices, or by the fact that the flow is slowed down downstream of the orifices, is deemed to be important [15][16][25][26][27][28]. Under the assumption of isenthalpic flow, this heat is supposed to remain within the fluid, contributing to increase its internal energy and therefore its temperature while the fluid expands, according to Eq. (2).

In order to calculate the temperature change in an isenthalpic expansion, let us consider the general formulation for the specific enthalpy as a function of the fluid temperature and pressure:

$$dh=\left(\frac{\partial h}{\partial T}\right)_p dT+\left(\frac{\partial h}{\partial p}\right)_T dp=c_p dT+\frac{1-\beta T}{\rho}dp \tag{3}$$

where c_p is the fluid heat capacity at constant pressure and β its volumetric thermal expansion coefficient, defined as:

$$\beta=\frac{1}{v}\left(\frac{\partial v}{\partial T}\right)_p=-\frac{1}{\rho}\left(\frac{\partial \rho}{\partial T}\right)_p \tag{4}$$

Note that the second term of the right hand side of Eq. (3) is null for an ideal gas (for which βT = 1), but cannot be neglected for a liquid. If the variation of the fluid properties (c_p, β and ρ) with respect to the pressure and temperature is known, Eq. (3) can be integrated taking into account that the final result is independent on the integration path [29]. This implies that it is possible to determine the fluid temperature after the expansion if the temperature upstream of the orifice and the pressure both upstream and downstream of the orifice are controlled. The particular procedure applied to calculate the temperature increase for the tested fuel is explained in Section 3.3.

3. EXPERIMENTAL TOOLS

3.1 Setup and hardware

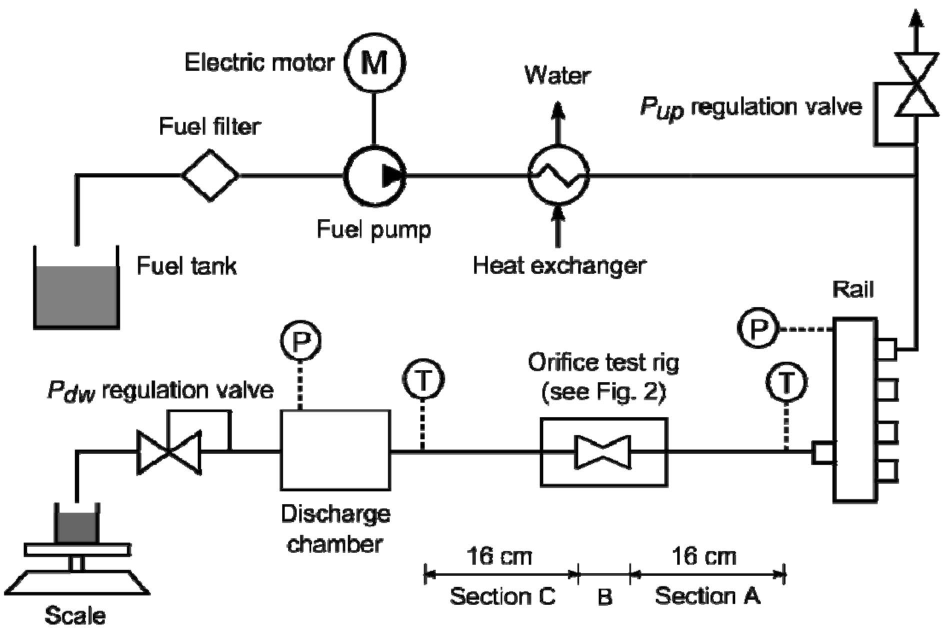

Figure 1: Experimental setup for the mass flow rate measurements. The thermocouple and pressure sensor locations are shown in the diagram.

Continuous flow was imposed through the restrictions under several conditions of controlled upstream and downstream pressure thanks to the experimental setup shown in Fig. 1. A fuel pump driven by an electric motor extracted fuel from a tank and rised its pressure after making it flow through a filter. The fuel was led to a commercial common-rail in which both temperature and pressure were controlled upstream of the rail by means of a water heat exchanger and a manual pressure relief valve, respectively. The orifice to be tested was fitted inside a test rig located downstream of the rail. The purpose of this test rig, specifically designed for each orifice, was to isolate the corresponding restriction so that fuel flowed in the adequate direction through the orifice and was not leaked through any other paths that could be possible during the normal operation of the complete injector. The test rig designed for the Denso G4S Outlet orifice is shown in Fig. 2 as a sample. The test rig for the measurements concerning the Bosch CRI 2.20 control orifices was already presented by the authors [14]. After the orifice, the fuel entered a discharge chamber where the pressure was controlled by means of another manual backpressure regulation valve placed downstream. The temperature jump across the orifice was determined from fuel temperature measurements carried out by type K thermocouples inserted at two locations of the high-pressure lines at which the flow was assumed to be develop and attain a similar velocity: right

Salvador, F.J., Gimeno, J., Carreres, M., Crialesi-Esposito, M., "Experimental assessment of the fuel heating and the validity of the assumption of adiabatic flow through the internal orifices of a diesel injector".

Fuel 188 (2017), pp. 442-451 (author version)

after the rail and before the discharge chamber (i.e., 16 cm upstream and downstream of the orifice). Finally, the fuel was injected into a glass in which the mass flow rate $\dot{m}$ could be measured in real time thanks to a scale connected to a computer. An air-conditioning unit was used in order to control the ambient temperature and keep it below the temperature upstream of the orifice so that, in case that the heat transfer with the surroundings was relevant, it would have taken place in the same direction (from the fluid to the surroundings) for all the tested operating conditions, thus enabling comparability among tests. The mass flow measurement was recorded for each tested condition after a short stabilization time by averaging it for a period of 80 seconds. This measurement allowed to determine the orifices discharge coefficient for the tested operating conditions, as stated by Eq. (5):

$$C_d = \frac{\dot{m}}{\dot{m}_{th}} = \frac{\dot{m}}{\rho A_o u_{th}} = \frac{\dot{m}}{A_o\sqrt{2\rho\left(p_{up} - p_{dw}\right)}} \tag{5}$$

where the theoretical flow velocity u_{th} is derived from Bernoulli's equation taking the assumption of negligible upstream velocity. The discharge coefficient strongly depends on the Reynolds number [30], defined as:

$$Re = \frac{\rho u_m D_o}{\mu} \tag{6}$$

where u_m is the flow mean velocity, determined from the mass flow rate through the continuity equation:

$$u_m = \frac{\dot{m}}{\rho A_o} \tag{7}$$

As explained in Section 3.2, several values of upstream and downstream pressure were considered in order to ensure that the experiments were performed on a wide range of *Re*, which led to the orifices being tested both in the laminar and the turbulent regimes.

Values of fuel density and viscosity in Eqs. (5) to (7) were taken at a mean temperature and a mean pressure by averaging the values of these conditions upstream and downstream of the orifice. More details on the fuel used in the investigation and its properties are given in Section 3.3.

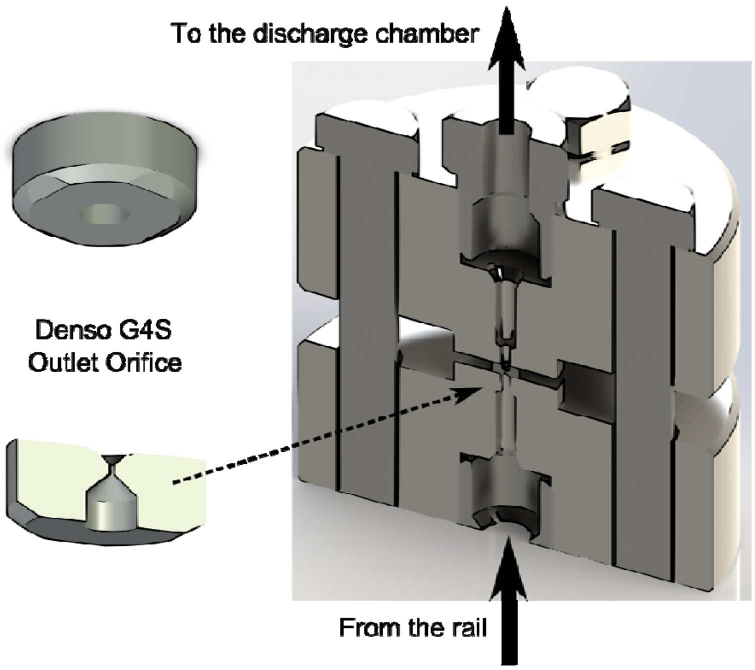

Figure 2: Orifice test rig for the Denso G4S Outlet orifice.

As already mentioned, the tests were carried out for five different control orifices belonging to two commercial common-rail injectors. The geometry of the orifices was determined by means of the silicone moulding and visualization technique explained by Macián et al. [31] and successfully applied in the literature [11][13]. A summary on the relevant geometrical parameters for each orifice is given in Table 1. It is important to note that three of the orifices (Bosch Outlet, Denso Inlet and Denso Control Valve) are cylindrical and therefore prone to cavitate [32]. This could affect the fuel heating upon expansion due to the different thermal behaviour of the vapour bubbles or to the enthalpy change associated to the phase change. The significance of this fact is analyzed in Section 4.

Injector	Orifice	D_i [µm]	D_o [µm]	L [mm]
Bosch CRI 2.20	Inlet	308	291	1.47
	Outlet	256	258	1.48
Denso G4S	Inlet	274	274	0.8
	Outlet	110	102	0.84
	Control Valve	199	198	0.75

Table 1: Tested orifices geometrical parameters.

3.2 Test Matrix

Table 2 depicts the operating conditions experimentally tested. Values of p_{up} range from 5 to 60 MPa. For each value of p_{up} tested, a sweep of p_{dw} was performed in order to ensure that each orifice worked for a wide range of Re values, so that all flow regimes (laminar, transitional and turbulent) are considered in the study. The maximum p_{dw} value tested was 12 MPa due to mechanical limitations of the discharge chamber.

p_{up} [MPa]	p_{dw} [MPa]
5	0.5 - 1 - 1.5 - 2 - 2.5 - 3 - 3.5 - 4 - 4.2 - 4.4 - 4.6 - 4.8
10	0.5 - 1 - 1.5 - 2 - 2.5 - 3 - 4 - 5 - 6 - 7 - 8 - 9
20, 30, 40, 50, 60	0.5 - 1 - 1.5 - 2 - 2.5 - 3 - 4 - 5 - 6 - 7 - 8 - 9 - 10 - 11 - 12

Table 2: Values of p_{dw} tested for each p_{up} considered.

3.3 Fuel

A standard B20 biodiesel blend (80% diesel, 20% rapeseed methyl ester) was chosen for the study. Eq. (3) highlighted the need of knowing the evolution of ρ, β and c_p with respect to the pressure and temperature in order to determine the theoretical temperature change after an isenthalpic expansion. Speed of sound measurements at different pressures and temperatures were carried out in order to determine the density following the procedure already validated by the authors [21][33]. The thermal expansion coefficient, β, was then determined through Eq. (4). On the other hand, the evolution of c_p with respect to the temperature was estimated from data of pure alkanes [34], whereas its variation with respect to the pressure was taken from similar hydrocarbons [35][36]. This assumption is not deemed to introduce a noticeable error, given the low variation of c_p for diesel fuels on the studied range of temperatures and pressures. With all, the map of specific enthalpy for the tested fuel was determined by applying Eq. (3) taking small variations of pressure and temperature instead of differentials (Fig. 3).

The specific enthalpy data were fitted to a polynomial equation:

$$h(T,p) = h_0 + h_T(T - T_0) + h_p(p - p_0) + h_{T2}(T - T_0)^2 + h_{Tp}(T - T_0)(p - p_0) + h_{p2}(p - p_0)^2 \quad (8)$$

The coefficients of Eq. (8) for the tested fuel are shown in Table 3, with a statistical R^2 value of 0.999967, which confirms the reliability of this regression. Eq. (8) can then be used to determine the theoretical temperature change for an isenthalpic expansion, solving the following expression for T_{dw}:

$$h(T_{dw}, p_{dw}) = h(T_{up}, p_{up}) \quad (9)$$

Fuel	h_T	h_p	$h_{T2}\cdot 10^3$	$h_{Tp}\cdot 10^5$	$h_{p2}\cdot 10^4$
B20	1.973502	0.913494	2.226358	7.336523	1.369723

Table 3: Eq. (8) correlation coefficients for the B20 fuel used in the experiments (T_0 = 298 K and p_0 = 0.1 MPa).

A look at Fig. 3 clearly shows that the fuel warms upon expansion, since isenthalpic lines need to be followed. For instance, it can be seen that an expansion from 60 MPa to atmospheric pressure with an inlet temperature of 280 K would lead to an outlet temperature of 308 K (ΔT = 28 K), or an expansion from 100 MPa to atmospheric pressure with an inlet temperature of 312 K would lead to an outlet temperature of 355 K (ΔT = 43 K).

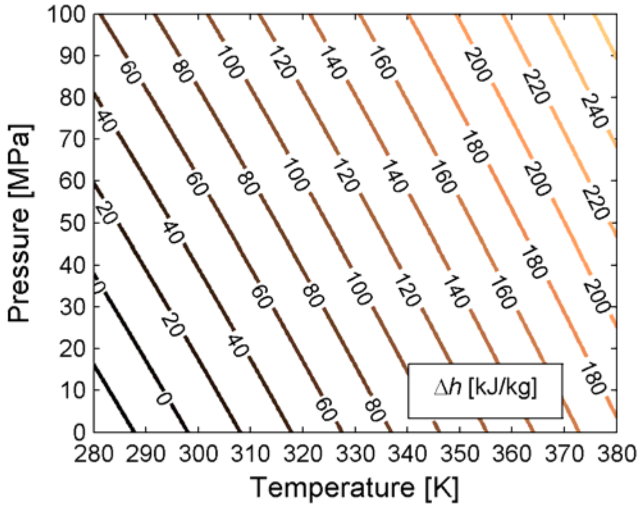

Figure 3: Fuel specific enthalpy evolution with respect to temperature and pressure. Reference: T_0 = 298 K; p_0 = 0.1 MPa.

4. RESULTS AND DISCUSSION

4.1 Orifices hydraulic behaviour

The continuous mass flow measurements explained in Section 3.1 made it possible to characterize the hydraulic behaviour of each of the tested orifices. Fig. 4 shows the C_d as a function of Re for the five orifices. Focusing on a given orifice, a theoretical asymptotic trend is clearly noticed, as expected according to the literature [30][37]. Fig. 4(a) shows that the Bosch Inlet orifice does not cavitate for any condition, since increasing Re always leads to higher values of C_d (in this case, the mass flow was always found to grow linearly with the square root of Δp). The rest of orifices, however, show branches of decreasing C_d, associated to the mass flow rate collapse noticed for each value of p_{up} from a given critical value of p_{dw} and below. This behaviour, attributed to cavitation [38], was expected for cylindrical orifices (recall Table 1) as already reported by the authors in several works concerning diesel injectors internal flow [11][13][17][18][23]. Fig. 4(b) also shows that, among all the cavitating orifices, the cavitation intensity is lower for the Denso Outlet orifice. This fact is also explained due to its geometry, since it is slightly conical (see Table 1). Table 4 shows details on some relevant parameters extracted from Fig. 4, such as the asymptotic $C_{d,max}$ to which each orifice tends and a Re_{crit} defined as the Re for which the exhibited C_d is 95% of $C_{d,max}$. This value is presented due to its importance in later sections, where it is used as the Re value that defines the transition from laminar to turbulent flow regime.

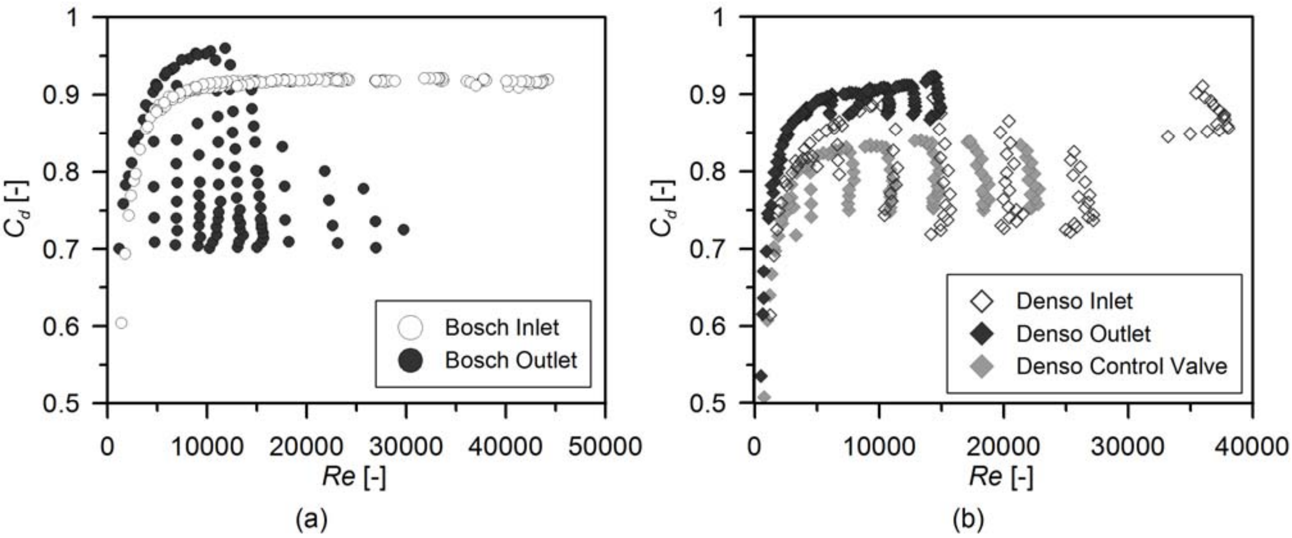

Figure 4: C_d as a function of Re for the control orifices of the Bosch injector (a) and the Denso injector (b).

Injector	Orifice	$C_{d,max}$ [-]	Re_{crit} [-]	Cavitation
Bosch CRI 2.20	Inlet	0.92	4600	No
	Outlet	0.96	5000	Yes
Denso G4S	Inlet	0.91	6800	Yes
	Outlet	0.92	4100	Yes
	Control Valve	0.84	3400	Yes

Table 4: Summary of the tested orifices hydraulic parameters.

Fig. 5(a) shows the experimental temperature increase (ΔT) as a function of the pressure drop (Δp) for two sample orifices (Denso Outlet and Denso Control Valve). The theoretical ΔT corresponding to an isenthalpic expansion is also shown in the figure. As it can be seen, the experimental ΔT registered was always lower than the theoretical one. Since the fuel was considerably warmer than the ambient in all cases, this means that heat was being transferred to the surroundings. However, deviations are low in the case of the Denso Control Valve orifice, where the flow practically behaved as if it were isenthalpic. For each operating condition tested, the deviation among the theoretical ΔT for an isenthalpic expansion and the experimentally registered ΔT was quantified as:

$$\varepsilon = \frac{\Delta T_{th} - \Delta T_{exp}}{\Delta T_{th}} \cdot 100\ (\%) \tag{10}$$

The evolution of ε against Δp for the three Denso injector orifices is shown in Fig. 5(b). Having a look at a given orifice, a decreasing trend is observed when Δp increases. In addition, the differences are bounded for each orifice as long as Δp is high enough. The most important differences in percentage terms take place for low values of Δp. In those cases, the flow may be laminar (the associated Re could be lower than the critical one), which means that viscous dissipation effects become relevant. These effects, located at the boundary layer, result in a decrease of the fuel velocity close to the wall (even though viscous heating induces higher fuel temperatures also close to the wall, which act in the sense of reducing the fuel viscosity thus damping the mentioned effect), thus increasing the fuel residence times in the channel. Hence, there may be enough time for the flow to lose heat to the surroundings.

In the case of the Denso Control Valve and Denso Inlet orifices, deviations are lower than 10% and 5%, respectively, except for the points at low pressure drop. Thus, it seems that the adiabatic assumption for the flow could be accurate enough for engineering purposes when dealing with these orifices as long as the pressure drop is not too low. On the contrary, differences become more important in the case of the Denso Outlet orifice, never being lower than 13%. This could be explained due to its lower diameter (102 μm): even though low diameters result in a lower effective surface for heat exchange, the reduction in cross-sectional area leads to a higher portion of the flow being affected by the boundary layer. The reduction of the flow velocity in this region results in higher fuel residence times that enhance heat transfer to the surroundings.

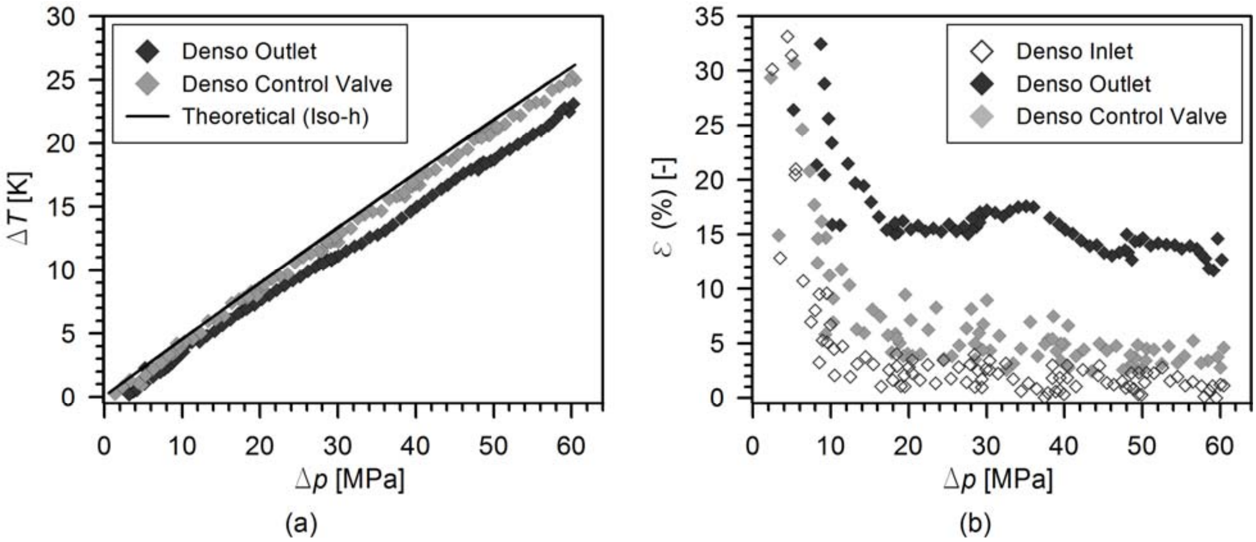

Figure 5: Temperature increase as a function of the pressure drop for two of the orifices tested (a). ε against the pressure drop for three of the orifices tested (b).

4.2 Derivation of a dimensionless parameter to quantify the proneness of an orifice to transfer heat with the surroundings

From the findings of Fig. 5, it seems that several parameters (such as flow velocity, viscosity - both of them linked through *Re* -, orifice diameter, etc.) are involved in the problem and it may be interesting to relate them in a single parameter to qualitatively quantify their effects in a combined way. This task is performed in this section.

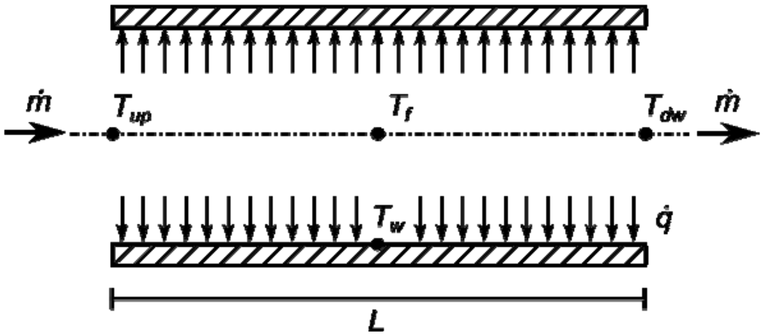

Figure 6: Scheme of flow through a circular duct with heat exchange to the surroundings.

Let us consider a fluid travelling through a channel of length L and perimeter P, as depicted in Fig. 6. The fluid enters the channel at a certain T_{up} temperature and leaves with a different temperature, T_{dw}. At any location inside the channel, the fluid is allowed to exchange heat with the surroundings since there may be a difference among its temperature, T_f, and the channel wall temperature, T_w. In these conditions, without any additional external work, the change in internal energy of the fluid must equal the heat transferred, which yields:

$$\dot{m}c_p\left(T_{dw} - T_{up}\right) = \alpha A_P\left(T_w - T_f\right) \tag{11}$$

where α is the convective heat transfer coefficient and A_P is the heat transfer area of the channel surface. It is then possible to define a dimensionless parameter (Ad) as the ratio among temperature changes:

$$Ad = \frac{\left(T_w - T_f\right)}{\left(T_{dw} - T_{up}\right)} = \frac{\dot{m}c_p}{\alpha A_P} \tag{12}$$

Ad may be referred to as *adiabatic* number and it quantifies the temperature difference needed among the channel wall and the fluid in order for the fluid to increase its temperature in 1 K at the channel outlet. In other words, *Ad* measures the proneness of a flow to retain the heat within itself instead of transferring it to the surroundings. Thus, the higher the value of *Ad*, the closer to the theoretical adiabatic condition the flow will behave. *Ad* may be expressed in terms of other dimensionless groups:

$$Ad = \frac{\dot{m}c_p}{\alpha A_P} = \frac{\rho A_o u_m c_p}{PL\alpha} = \frac{1}{4}\frac{D}{L}\frac{\rho u_m c_p}{\alpha} = \frac{1}{4}\frac{D}{L}St^{-1} \tag{13}$$

where the concept of hydraulic diameter (equal to the channel diameter in a circular channel) as the ratio among the cross-sectional area A_o and the perimeter P of the channel has been used. Hence, *Ad* is directly related to the diameter-to-length ratio of the channel and to the Stanton number, *St*, which relates the heat transferred into a fluid through convection to its heat capacity. *St* can also be expressed as a function of *Nu*, *Pr* and *Re* so that:

$$Ad = \frac{1}{4}\frac{D}{L}St^{-1} = \frac{1}{4}\frac{D}{L}\frac{PrRe}{Nu} \tag{14}$$

4.3 Evaluation of the Ad number for the tested orifices

As pointed out by Eq. (14), the derivation of *Ad* is consistent with the findings reported in Section 4.1: heat transfer to the surroundings is enhanced by low values of *Re* and low diameters for a given channel length. In this section, *Ad* is evaluated for each of the tested conditions for all the orifices in order to assess its usefulness. Since the thermocouples of the experimental setup described in Section 3.1 were located in the high pressure lines at a certain distance (16 cm) upstream and downstream of the orifice (recall Fig. 1), and the diameter of these lines (5 mm) differs from the orifices diameters, *Ad* has been evaluated taking into account three different sections (labelled in Fig. 1):

- Section A: from the thermocouple upstream of the orifice to the entrance of the orifice test rig.
- Section B: from the entrance of the orifice test rig to its outlet.
- Section C: from the orifices test rig outlet to the location of the thermocouple downstream of the orifice.

Attending to the two ΔT involved in the generic definition of *Ad*, its corresponding value among Sections A and C can be established from the following expression:

$$\frac{1}{Ad} = \frac{\left(T_{dw} - T_{up}\right)}{\left(T_w - T_f\right)} = \frac{\Delta T_C + \Delta T_B + \Delta T_A}{\left(T_w - T_f\right)} = \frac{1}{Ad_A} + \frac{1}{Ad_B} + \frac{1}{Ad_C} \tag{15}$$

Therefore:

$$Ad = \frac{1}{\sum \frac{1}{Ad_i}} = \frac{1}{\sum\left(4\frac{L_i}{D_i}\frac{Nu_i}{Pr_i Re_i}\right)} \tag{16}$$

For each value of Δp tested, Re_i can be evaluated from the continuous mass flow measurements. Pr_i, in turn, can be easily calculated from the fuel properties:

$$Pr_i = \frac{\mu_i c_{p_i}}{k_i} \tag{17}$$

where *k* is the fuel thermal conductivity, which for the present investigation was taken from a generic diesel fuel as reported in [29]. With regard to the Nusselt number, empirical correlations to relate it to *Re* and *Pr* are readily available in the literature. In the present work, the correlation introduced by Sieder & Tate [39] was used for laminar flow:

$$Nu = 1.86\left(\frac{D}{L}RePr\right)^{1/3}\left(\frac{\mu_b}{\mu_w}\right)^{0.14} \tag{18}$$

where the last term, relating the fluid bulk viscosity (μ_b) to the fuel viscosity at the wall (μ_w), has been neglected. In the case of turbulent flow, the correlation defined by Nusselt [40], valid for short tubes ($10 < L/D < 400$), was used instead:

$$Nu = 0.036Re^{0.8}Pr^{1/3}\left(\frac{D}{L}\right)^{1/18} \tag{19}$$

Eqs. (17) to (19) highlight the relevance of the fuel properties in the evaluation of *Ad* through *Re*, *Pr* and *Nu*. Given the important changes in fuel temperature and pressure through sections A to C in the experiments, the fuel properties involved (ρ, μ, c_p and k) have been evaluated accordingly, as stated in Table 5. The criteria for the evaluation of *Nu* are also shown in the table. As implied by the table, the flow has been assumed to be laminar along sections A and C for all the orifices. This assumption is based on the low values of *Re* found from the measurements of these locations: $Re <$ 400 for the Denso outlet orifice and $Re < 2600$ for the Bosch inlet orifice regardless the pressure conditions tested. In the case of section B, some operating conditions lead to $Re < Re_{crit}$ (laminar flow) and some others to $Re > Re_{crit}$ (turbulent flow). Consequently, there may be cases in which the flow through sections A to C is a mixture of laminar and turbulent flow. All the calculations concerning heat transfer parameters were carried out in accordance to this fact. Mean values of *Nu* are thus considered for each section through the application of Eqs. (18) or (19).

Section	Fuel properties	*Nu* correlation
A	Evaluated for p_{up} and T_{up}	Laminar flow
B	Evaluated for the average values of p and T upstream and downstream of the orifice	Laminar flow if $Re < Re_{crit}$ Turbulent flow if $Re > Re_{crit}$
C	Evaluated for p_{dw} and T_{dw}	Laminar flow

Table 5: Criteria for the evaluation of the fuel properties and *Nu* at the different sections of the experimental setup.

Fig. 7 shows the evolution of ε against *Ad* for all the tested points corresponding to the Bosch Outlet orifice and the Denso Control Valve orifice. A distinction is made among the operating points leading to cavitating conditions and those corresponding to non-cavitating conditions. Focusing on the behaviour for non-cavitating conditions, a decreasing trend of the deviation with the *Ad* number is clearly observed for both cases. This fact agrees with the purpose of the *Ad* number definition and is expected since the lowest values of *Ad* correspond to low values of *Re* (Eq. (14)), for which the flow along the orifice is laminar (recall Fig. 4). In the experiments, these points are found for the lowest Δp values tested. In these conditions, the flow velocity is reduced, increasing the fuel residence time and allowing heat exchange with the surroundings. On the other hand, *Ad* increases for higher values of Δp, for which the flow gets turbulent and its velocity is increased, reducing the available time to transfer heat to the surroundings. With all, it can be seen that the operating conditions leading to *Ad* values higher than 4 lead in both cases to relatively low deviations compared to the theoretical ΔT corresponding to an isenthalpic expansion. Indeed, these deviations are bounded within a 10% margin, making it possible to state that the flow nearly behaves as if it were adiabatic. In addition, ε is generally lower for the Bosch Outlet orifice than for the Denso Control Valve orifice. This is consistent with the *Ad* definition since the former generally leads to higher values of *Ad* than the latter due to its higher diameter.

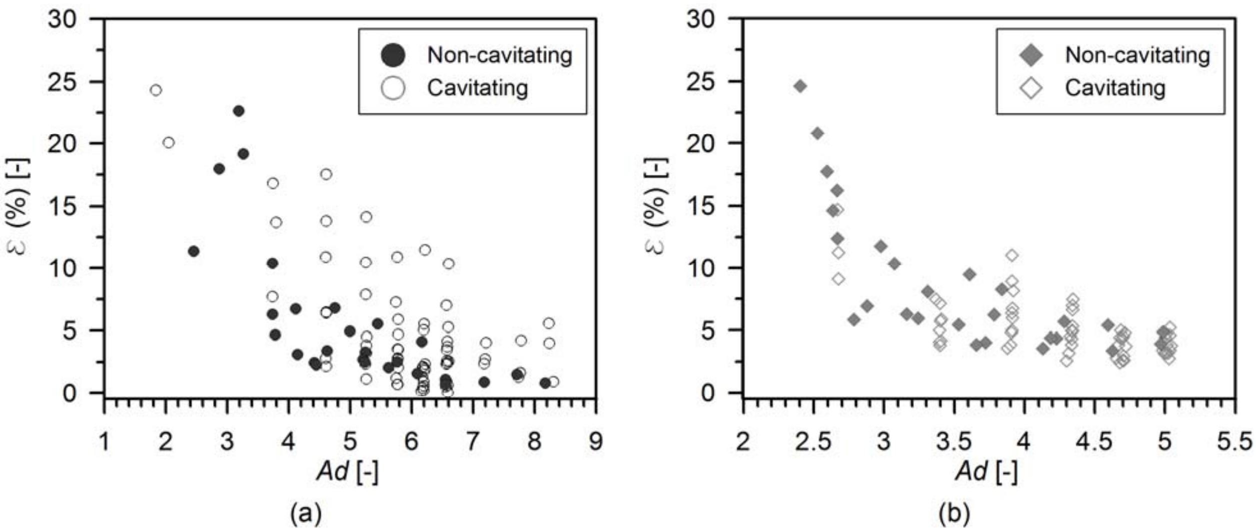

Figure 7: ε against the *Ad* number for the Bosch Outlet orifice (a) and the Denso Control Valve orifice (b). Points corresponding to both cavitating and non-cavitating conditions are represented.

Having a look at the cavitating conditions in Fig. 7, the observed values of ε are more scattered than those reported for non-cavitating conditions. There seem to be groups of operating conditions that lead to the same value of *Ad* but register different levels of deviation (for instance, for $Ad \approx 5.2$ in the case of the Bosch Outlet orifice, there are operating conditions for which the deviation ranges among 2 and 15%). Each of these groups correspond to a given value of upstream pressure. Hence, for a given group, the deviation depends on the cavitation intensity (i.e. the lower the downstream pressure). In order to better analyse the role of cavitation in this matter, let us introduce the cavitation number *CN* defined by Soteriou et al. [41]:

Salvador, F.J., Gimeno, J., Carreres, M., Crialesi-Esposito, M., "Experimental assessment of the fuel heating and the validity of the assumption of adiabatic flow through the internal orifices of a diesel injector".

Fuel 188 (2017), pp. 442-451 (author version)

$$CN = \frac{p_{up} - p_{dw}}{p_{dw} - p_v} \approx \frac{p_{up} - p_{dw}}{p_{dw}} \qquad (20)$$

where p_v is the vapour pressure. This number quantifies the proneness of an orifice to cavitate. Once cavitation conditions are achieved, the cavitation intensity is higher as *CN* grows.

Fig. 8 depicts ε against *CN* for the Bosch Outlet orifice. As it may be seen, this magnitude generally grows the higher the cavitation intensity. Therefore, the flow behaviour importantly departs from being nearly isenthalpic. This fact should not be attributed to the local cooling associated to the enthalpy of phase change, since other authors have shown its relatively low importance (in the order of tenths of a degree) [42]. However, it might be explained considering that the heat transfer parameters associated to the vapour bubbles (specifically the convective heat transfer coefficient, α) importantly differ from those of the liquid phase. Indeed, Bergman et al. [43] reported an increase in α with the appearing vapour bubbles that would lead to lower effective *Ad* values, supporting the higher deviations observed in Fig. 7 for cavitating conditions. These considerations were not taken into account in the evaluation of *Ad*, given the difficulty to quantify the dependency of α with the cavitation intensity, but would act in the sense of collapsing the points corresponding to cavitating conditions with the ones corresponding to non-cavitating conditions shown in Fig. 7.

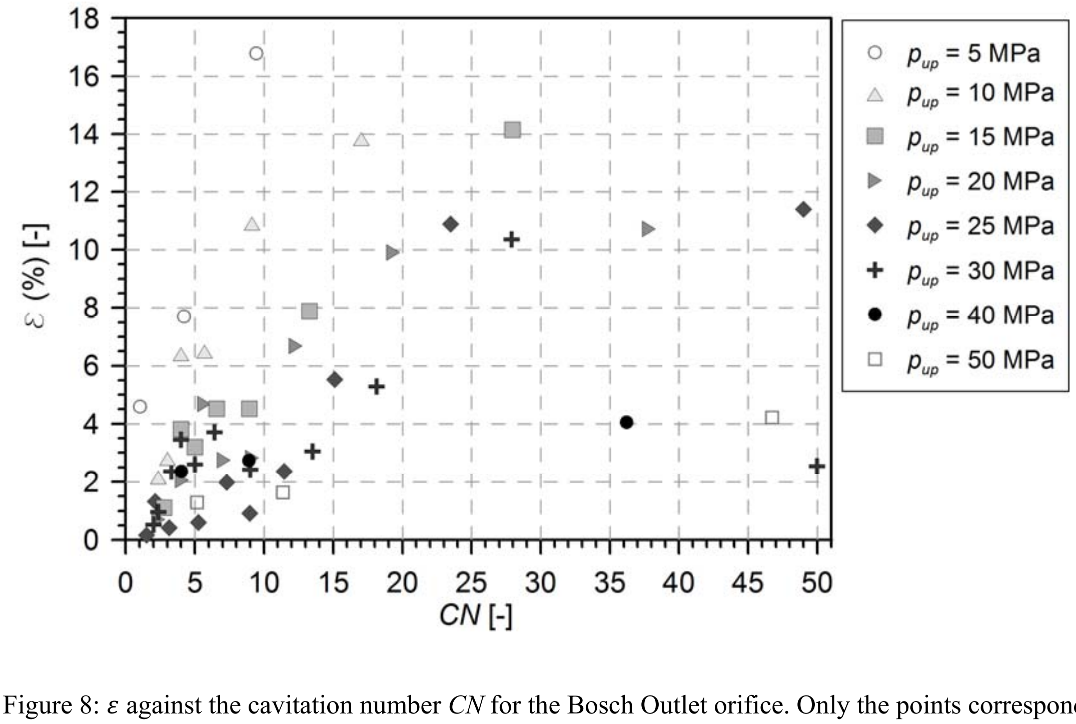

Figure 8: ε against the cavitation number *CN* for the Bosch Outlet orifice. Only the points corresponding to cavitating conditions are represented.

In addition, for a given value of CN, the deviations are less important the higher the upstream pressure p_{up}. This is also consistent with the commented findings regarding Δp and *Ad*.

At this point, it is interesting to check the behaviour of all the orifices jointly. Fig. 9 shows ε plotted against *Ad* for all the orifices tested. Given the remarks on cavitating conditions, only the points corresponding to non-cavitating conditions are represented. The same decreasing trend that was reported for a given orifice is noticed. Given the *Ad* number definition, the orifices are effectively sorted by their outlet diameters (recall Table 1): the Denso Outlet orifice leads to lower values of *Ad*, followed by the Denso Control Valve orifice, Bosch Outlet, Denso Inlet and Bosch Inlet, in this order. This scaling with the diameter was expected as explained in Section 4.1 in view of Fig. 5. Thus, orifices that lead to low values of *Ad*, even for the higher Δp values tested, present high deviations with respect to the theoretical isenthalpic expansion. Hence, the deviations found for the Denso Outlet orifice are higher than 13% even for its higher values of *Ad*. On the contrary, since the conditions tested for the Bosch Inlet orifice never lead to low values of *Ad*, their deviations are bounded. In addition, the points of Fig. 9 corresponding to different orifices tend to collapse for a given value of *Ad*, which highlights the usefulness of this number. As it was found for a given orifice, it is possible to state in a more general way that the flow through orifices leading to high average values of *Ad* behaves in a nearly adiabatic manner (for instance, *Ad* values higher than 4 keep the deviations bounded within a 10% margin).

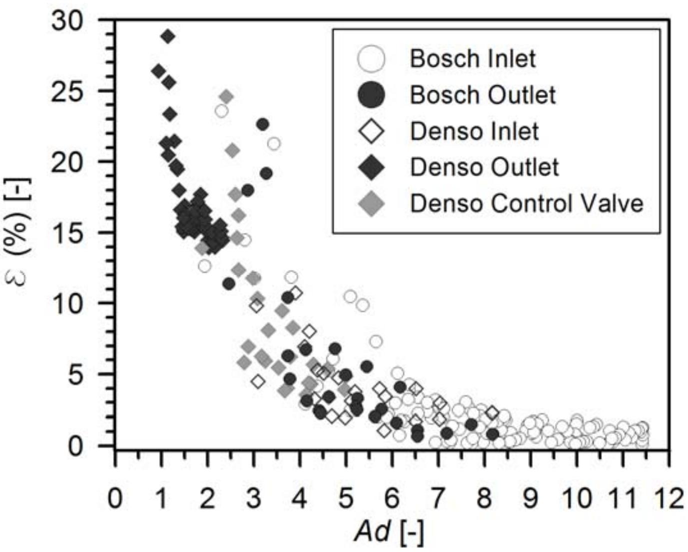

Figure 9: ε against the *Ad* number for all orifices. Only the points corresponding to non-cavitating conditions are represented.

With all, a dimensionless number to determine in a qualitative way the proneness of the flow through a diesel injector internal orifice to exchange heat with the surroundings has been defined. It is important to state that the results here presented in terms of *Ad* should not be relied on quantitatively, given the nature of the experiments. On the one hand, these experiments were carried out at a certain ambient temperature. On the other hand, the temperatures upstream and downstream of the orifice were measured at a certain distance from the orifice itself. Thus, most of the heat transfer effectively took place in the high pressure lines connecting the orifice to the rail and the discharge chamber. However, the validity of the methodology of this study is yet not compromised since the flow through these lines was still governed by the restriction imposed by each orifice.

5. CONCLUSIONS

In this work, the proneness of the flow through diesel injector internal orifices to resemble adiabatic flow was assessed experimentally by carrying out measurements on 5 different orifices corresponding to 2 commercial injectors. The tests consisted on measuring the flow rate and temperature established upon an expansion through the orifice, by controlling the pressure conditions upstream and downstream of the orifices. The main conclusions of the study are summarized in the following points:

- In adiabatic conditions and among two locations where the changes in flow velocity are not relevant, diesel fuel warms upon expansion through an injector internal orifice, as deduced from the null enthalpy change.
- The proneness of an orifice to exchange heat with the surroundings is directly related to the *Re* and flow regime. Low *Re* values imply relatively low flow velocities, which increase the fuel residence times in the duct, thus allowing heat transfer to take place. On the contrary, high flow velocities are established for high values of *Re*, making it possible to neglect the heat transfer and to assume that all the heat internally generated remains within the fluid raising its temperature. Therefore, low pressure drops through an orifice induce a higher interaction with the ambient than high pressure drops.
- The diameter also influences the tendency of a given orifice to transfer heat to the surroundings, and not only due to its impact through *Re*. This is explained since, for a given channel length, a lower diameter implies a relatively higher proportion of the flow being in contact with the channel wall, which directly favours heat losses to the ambient. In addition, these wall effects also imply the existence of a boundary layer where flow effective velocity is importantly reduced by viscosity, also increasing the fuel residence times leading to heat transfer.
- It is possible to define a dimensionless parameter to qualitatively assess the proneness of the flow through an orifice to exchange heat with the surroundings depending on the pressure drop driving the flow. The definition

of such a parameter in this work (*Ad*) comprises all the previously stated effects for non-cavitating flows, and has made it possible to establish that heat transfer should not be neglected for orifices with small diameter, regardless the flow conditions. On the contrary, the flow can be treated as nearly adiabatic for orifices with high diameter, regardless the flow conditions. With all, any combination of orifice diameter and pressure conditions can be assessed beforehand by means of the *Ad* number.

- With regard to cavitating conditions, the difficulty in obtaining the variation of the heat transfer coefficient with the appearing vapour bubbles does not enable the quantitative evaluation of the *Ad* number. However, it has been checked that the flow gradually departs from being adiabatic as the cavitation intensity grows. This is consistent with the definition of *Ad* since the heat transfer coefficient is deemed to increase as cavitation gets more important. Therefore, the conclusions of the study may be generally extended to cavitating conditions.

ACKNOWLEDGEMENTS

This work was partly sponsored by "Ministerio de Economía y Competitividad", of the Spanish government, in the frame of the project "Estudio de la interacción chorro-pared en condiciones realistas de motor", reference TRA2015-67679-c2-1-R. This support is gratefully acknowledged by the authors.

The authors would also like to thank José Enrique del Rey, Edison Díaz and Léo Thiercelin for their technical help on the experimental setup and their support during the measurements.

REFERENCES

[1] Lefèbvre, A.H., Atomization and Sprays, Hemisphere, 1989, ISBN 0891166033.

[2] Payri, R., Salvador, F.J., Gimeno, J., Soare, V. Determination of Diesel sprays characteristics in real engine in-cylinder air density and pressure conditions, Journal of Mechanical Science and Technology, 19 (2005), pp. 2040-2052.

[3] Lee, C.S., Lee, K.H., Reitz, R.D., Park, S.W., Effect of split injection on the macroscopic development and atomization characteristics of a Diesel spray injected through a common-rail system, Atomization and Sprays, 16(5) (2006), pp. 543-562.

[4] Som, S., Ramirez, A.I., Longman, D.E., Aggarwal, S.K., Effect of nozzle orifice geometry on spray, combustion, and emission characteristics under diesel engine conditions, Fuel, 90 (2011), pp. 1267-1276.

[5] Park, S.H., Yoon, S.H., Lee, C.S., Effects of multiple-injection strategies on overall spray behavior, combustion, and emissions reduction characteristics of biodiesel fuel, Applied Energy, 88(1) (2011), pp. 88-98.

[6] Agarwal, A.H., Dhar, A., Gupta, J.G., Kim, W.I., et al., Effect of fuel injection pressure and injection timing of Karanja biodiesel blends on fuel spray, engine performance, emissions and combustion characteristics, Energy Conversion and Management, 91 (2015), pp. 302-314.

[7] Gumus, M., Sayin, C., Canakci, M., The impact of fuel injection pressure on the exhaust emissions of a direct injection diesel engine fueled with biodiesel-diesel fuel blends, Fuel, 95(1) (2015), pp. 486-494.

[8] Wang, X., Huang, Z., Zhang, W., Kuti, O-A., Nishida, K., Effects of ultra-high injection pressure and micro-hole nozzle on flame structure and soot formation of impinging diesel spray, Fuel, 90 (2011), pp. 1172-1180.

[9] Seykens, X.L.J., Somers, L.M.T., Baert, R.S.G., Detailed modelling of common rail fuel injection process, Journal of Middle European Construction and Design of Cars (MECCA), 3 (2005), pp. 30-39.

[10] Catania, A.E., Ferrari, A., Spessa, E., Temperature variations in the simulation of high-pressure injection-system transient flows under cavitation, International Journal of Heat and Mass Transfer, 51 (2008), pp. 2090-2107.

[11] Payri, R., Salvador, F.J., Martí-Aldaraví, P., Martínez-López, J., Using one-dimensional modeling to analyse the influence of the use of biodiesels on the dynamic behavior of solenoid-operated injectors in common rail systems: Detailed injection system model, Energy Conversion and Management, 54 (2012), pp. 90-99.

[12] Salvador, F.J., Gimeno, J., De la Morena, J., Carreres, M., Using one-dimensional modeling to analyse the influence of the use of biodiesels on the dynamic behavior of solenoid-operated injectors in common rail systems: Results of the simulations and discussion, Energy Conversion and Management, 54 (2012), pp. 122-132.

[13] Salvador, F.J., Plazas, A.H., Gimeno, J., Carreres, M., Complete modelling of a piezo actuator last-generation injector for diesel injection systems, International Journal of Engine Research, 15(1) (2014), pp. 3-19.

[14] Payri, R., Salvador, F.J., Carreres, M., De la Morena, J., Fuel temperature influence on the performance of a last generation common-rail diesel ballistic injector. Part II: 1D model development, validation and analysis, Energy Conversion and Management, 114 (2016), pp. 376-391.

[15] Theodorakakos, A., Strotos, G., Mitroglou, N., Atkin, C., Gavaises, M., Friction-induced heating in nozzle hole micro-channels under extreme fuel pressurization, Fuel, 123 (2014), pp. 143-150.

[16] Strotos, G., Koukouvinis, P., Theodorakakos, A., Gavaises, M., Bergeles, G., Transient heating effects in high pressure Diesel injector nozzles, International Journal of Heat and Fluid Flow, 51 (2015), pp. 257-267.

[17] Desantes, J.M., Salvador, F.J., Carreres, M., Martínez-López, J., Large-eddy simulation analysis of the influence of the needle lift on the cavitation in diesel injector nozzles, Proceedings of the Institution of Mechanical Engineers, Part D: Journal of Automobile Engineering, 229(4) (2014), pp. 407-423.

[18] Salvador, F.J., Carreres, M., Jaramillo, D., Martínez-López, J., Analysis of the combined effect of hydrogrinding process and inclination angle on hydraulic performance of diesel injection nozzles, Energy Conversion and Management, 105 (2015), pp. 1352-1365.

[19] Rodríguez-Anton, L., Casanova-Kindelan, J., Tardajos, G., High Pressure Physical Properties of Fluids used in Diesel Injection Systems, SAE Technical Paper 2000-01-2046, 2000.

[20] Dernotte, J., Hespel, C., Houillé, S., Foucher, F., et al., Influence of fuel properties on the diesel injection process in nonvaporizing conditions, Atomization and Sprays, 22(6) (2012), pp. 461-492.

[21] Payri, R., Salvador, F.J., Gimeno, J., Bracho, G., The effect of temperature and pressure on thermodynamic properties of diesel and biodiesel fuels, Fuel, 90 (2011), pp. 1172-1180.

[22] Park, Y., Hwang, J., Bae, C., Kim, K., et al., Effects of diesel fuel temperature on fuel flow and spray characteristics, Fuel, 162 (2015), pp. 1-7.

[23] Salvador, F.J., Gimeno, J., Carreres, M., Crialesi-Esposito, M., Fuel temperature influence on the performance of a last generation common-rail diesel ballistic injector. Part I: Experimental mass flow rate measurements and discussion, Energy Conversion and Management, 114 (2016), pp.364-375.

[24] Matsumoto, S., Klose, C., Schneider, J., Nakane, N., et al., 4th Generation Diesel Common Rail System: Realizing Ideal Structure Function for Diesel Engine, SAE Technical Paper 2013-01-1590, 2013.

[25] Xu, B., Ooi, K.T., Mavriplis, C., Zaghloul, M.E., Evaluation of viscous dissipation in liquid flow in microchannels, Journal of Micromechanics and Microengineering, 13 (2003), pp. 53-57.

[26] Koo, J., Kleinstreuer, C., Viscous dissipation effects in microtubes and microchannels, International Journal of Heat and Mass Transfer, 47 (2004), pp. 3159-3169.

[27] Morini, G.L., Viscous heating in liquid flos in micro-channels, International Journal of Heat and Mass Transfer, 48 (2005), pp. 3637-3647.

[28] Han, D., Lee, K., Viscous dissipation in micro-channels, Journal of Mechanical Science and Technology, 21 (2007), pp. 2244-2249.

[29] Kolev, N.I., Multiphase flow dynamics 3: turbulence, gas absorption and release, diesel fuel properties, Springer Verlag, 2002, ISBN 978-3-540-71443-9.

[30] Lichtarowicz, A.K., Duggins, R.K., Markland, E., Discharge coefficients for incompressible non-cavitating flow through long orifices, Journal of Mechanical Engineering Science, 7(2) (1965), pp. 210-219.

[31] Macián, V., Bermúdez, V., Payri, R., Gimeno, J., New technique for the determination of internal geometry of a diesel nozzle with the use of silicone methodology, Experimental Techniques, 27(2) (2003), pp. 39-43.

[32] Salvador, F.J., Martínez-López, J., Caballer, M., de Alfonso, C., Study of the needle lift on the internal flow and cavitation phenomenon in diesel injector nozzles by CFD using RANS methods, Energy Conversion and Management, 66 (2013), pp. 246-256.

[33] Desantes, J.M., Salvador, F.J., Carreres, M., Jaramillo, D., Experimental Characterization of the Thermodynamic Properties of Diesel Fuels Over a Wide Range of Pressures and Temperatures, SAE International Journal of Fuels and Lubricants, 8(1) (2015), pp. 190-199.

[34] Huang, D., Simon, S.L., McKenna, G.B., Chain length dependence of the thermodynamic properties of linear and cyclic alkanes and polymers, The Journal of Chemical Physics, 122 (2005), 084907.

[35] Bell, I.H., Wronski, J., Quoilin, S., Lemort, V., Pure and Pseudo-pure Fluid Thermophysical Property Evaluation and the Open-Source Thermophysical Property Library Coolprop, Industrial & Engineering Chemistry Research, 53(6) (2014), pp. 2498-2508.

[36] Chorazewski, M., Dergal, F., Sawaya, T., Mokbel, I., et al., Thermophysical properties of Normafluid (ISO 4113) over wide pressure and temperature ranges, Fuel, 105 (2013), pp. 440-450.

[37] Desantes, J.M., López, J.J., Carreres, M., López-Pintor, D., Characterization and prediction of the discharge coefficient of non-cavitating diesel injection nozzles, Fuel, 184 (2016), pp. 371-381.

[38] Nurick, W.H., Orifice cavitation and its effect on spray mixing, Journal of Fluids Engineering, 98(4) (1976), pp. 681-687.

[39] Sieder, E.N., Tate, G.E., Heat Transfer and Pressure Drop of Liquids in Tubes, Industrial and Engineering Chemistry, 28(12) (1936), pp. 1429-1435.

[40] Nusselt, W., Der Wärmeaustausch zwischen Wand und Wasser im Rohr, Forschung auf dem Gebiet des Ingenieurwesens A, 2(9) (1931), pp. 309-313.

[41] Soteriou, C., Andrews, R., Smith, M., Direct Injection Diesel Sprays and the Effect of Cavitation and Hydraulic Flip on Atomization, SAE Technical Paper 950080 (1995).

[42] Franc, J.P., The Rayleigh-Plesset equation: a simple and powerful tool to understand various aspects of cavitation, In "Fluid Dynamics of Cavitation and Cavitating Turbopumps", pp. 1-41, Springer Vienna, 2007, ISBN 978-3-211-76668-2.

[43] Bergman, T.L., Lavine, A.S., Incropera, F.P., DeWitt, D.P., Fundamentals of Heat and Mass Transfer, Wiley John & Sons, 2011, ISBN 978-0470917855.